Comparison and Detailing of Vertical Dynamic Models and Their Application Contexts

Paulo Henrique Dayrell Drummond de Oliveira
R&D Jr. Engineer, Prometeon Tyre Group

Anderson Muniz Calhabeu
Open Innovation Coordinator, Prometeon Tyre Group

Vitor Mainenti Leal Lopes
Professor, Universidade Federal de Juiz de Fora

ABSTRACT

The response of an automobile when excited by the highway rugosity and a non-uniformity between the tyre-wheel assembly can be evaluated through masses-springs-dampers models. These models calculate the degrees of freedom (DOF) of the represented displacements and its variation over time. With them, a possibility is introduced to analyze comfort, stability, and wheel travel, which are important parameters to vehicle dynamicists compare with the design requirements. Computer-aided engineering technology, such as the robust multibody dynamics technique, come into view as extremely useful tools with elevated application potential. However, they are affected by high preprocessing time and the necessity of a large amount of data as input. With that in mind, models with fewer DOF presents themselves as interesting on conceptual stage of a vehicle design, since them are much less data and effort demanding, besides of being easily applied. Also, they are crucial to understand basic concepts of mechanical vibrations applied to suspension calibration. In this paper, a comparative study with an application context detailing is made with 4 known vertical dynamics models: the 1 DOF, quarter-car with 2 DOF, half-car with 4 DOF and finally the full-car with 7 DOF.

INTRODUCTION

MODELLING – As it is often the case in the field of engineering, many problems does not allow, due its complexity, a precise formulation nor an exact solution, mainly because the behaviors of the physical system are typically governed by ordinary or partial differential equations (DE), which do not commonly have a straightforward solution. Currently, the technique of Multibody Dynamics (MBD) serves as the reference in terms of representation and correlation with reality to solve the equations of motion of complex models. However, the models with reduced DOF, such as the ones treated in the present paper, are highly effective for initial exploration with numerical integration, mechanical vibration, algorithms, vertical dynamics/ride and so on.

In the industry of vehicles design, the MBD is the simulation method implemented widely in terms of vehicle dynamics analysis. Inside student competitions, recreational designs, simpler vehicles architectures and learning environments, the vertical models from 1 to 7 DOF are notably a good alternative, since those contexts have limited resources of data, softwares and demand for complexity altogether.

RIDE – Vertical dynamics is a subfield of vehicle dynamics that focuses on analyzing the response of masses in terms of displacements, velocities, and accelerations after passing through a road with high undulations (base excitation) or during an unbalanced tyre-wheel assembly (unbalanced rotation). The suspension plays a crucial role in filtering and controlling the movements of both the sprung and unsprung masses, dissipating energy and influencing transmissibility. Furthermore, the coupling of vibration modes contributes to the overall behavior, making it a significant aspect to consider in vehicle design.

OBJECTIVES

This paper aims to study how the response of 4 vertical dynamics models compare to each other, allowing a good definition of which context a more complex model is needed and defining the limitations of the models with fewer DOF. Additionally, a description of the characteristics of each model, not only in the conceptual viewpoint, but also in mathematical terms, was included.

All the models here treated are not, in any way, new to the studies of vehicle dynamics. However, a comparison between all of them was not found clear and direct. The concrete knowledge of the performance of each model is very helpful, especially during the phase of decision of

which model is appropriate to have a coherent response without introducing unnecessary complexity.

In terms of comparison, all the models must be evaluated with inputs of road excitation, such as harmonic (sinusoidal) and transient (step) excitations, and in parallel, outside the time domain, the model's natural frequencies must be evaluated through modal analysis. This comprehensive evaluation approach provides a robust basis for comparing the models.

1 DOF MODEL

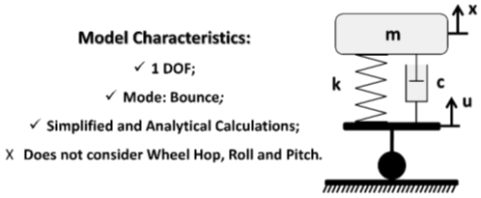

Figure 1. 1/8 Model

ALSO KNOWN AS EIGHTH-CAR [1] – With 1 DOF it is possible to describe how a suspension system work in the simplest approach. This simple linear model represents a single sprung mass degree of freedom of vertical translation named bounce, considering a rigid tyre that do not detach from the road, likewise all the other models. The eighth-car consists of a mass-spring-damper (MSD) system, that considers only one of the eight masses of a common vehicle (4 sprung masses and 4 unsprung masses, with each supported by one tyre).

Figure 1 illustrates this model showing suspension parameters such as suspension stiffness k (N/m), suspension damping $(N.s/m)$, and the sprung mass m (kg).

It is important to note that both suspension stiffness and damping are measured at the wheel center, and therefore, these values do not directly correlate with the spring rate and damping coefficient of the shock absorbers. The concept of mechanical advantage is utilized based on the installation ratio (IR) of the shocks on the suspension arms. Therefore, for a spring rate k_s, wheel center rate of k_w, and with an installation ratio IR, the relationship is given by Equation 1.

$$k_w = k_s \cdot IR^2 \tag{1}$$

The Figure 2 illustrates the concept of mechanical and geometric advantage of the suspension lever without angle of attack, with F_w as wheel forces and F_s spring forces.

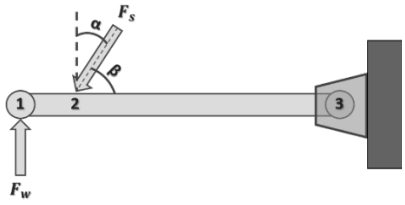

Figure 2. Suspension Arm Lever

The same principle is extended to all the other models, which also consider the wheel center rate. Since the models are linear and have constant stiffness, it is assumed that the geometric rate, as described in reference [2] and defined as the derivative of the installation ratio with respect to suspension travel, is zero.

Specifically in this model, to compensate for the lack of tire contribution to ride comfort, the concept of ride rate described in reference [3] and defined in Equation 2 can be utilized. This parameter combines the tire vertical stiffness (k_t) with the suspension spring stiffness in series, resulting in a less stiff value that replaces the stiffness (k) shown in Figure 1, because of the series association.

$$RR = \frac{k_w \cdot k_t}{k_w + k_t} \tag{2}$$

2 DOF MODELS

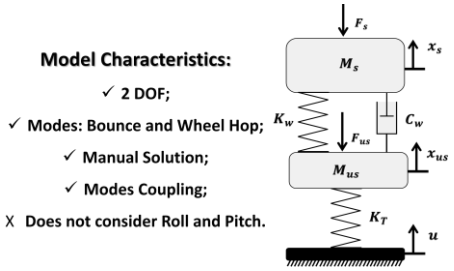

Figure 3. 1/4 Model

ALSO KNOWN AS QUARTER-CAR – The classical application of the 2 DOF model is depicted in Figure 3, where half of the sprung mass and half of the unsprung mass of the axle are analyzed. Two quarter-car models are required to analyze the front and rear suspensions separately, applying the corresponding values to the respective axle under analysis.

The 2 DOF model introduces the tyre vertical stiffness, allowing the unsprung mass to vibrate on the parallel spring association of the suspension and the tyre. Therefore, the quarter-car is the first model to present mode coupling: the resonance of the unsprung mass vibration influences the sprung mass.

In this paper, the subscription of the parameters "s" always refers to spring or sprung, "us" or simply "u" to unsprung, "T" for tyre, "w" for the wheel center equivalent. Masses, springs, and dampers are always M, K, C, respectively. The axles are referred as "F" for the front, "R" for the rear, the sides are referred with "L" as left and "R" as right. At last, "u" is always the road input.

4 DOF MODEL

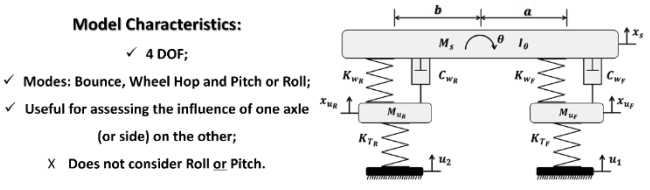

Figure 4. 1/2 Model

ALSO KNOWN AS HALF-CAR – The 4 DOF model have the peculiarity of allowing its interpretation based on 2 different planes: the frontal plane, which defines an analysis

of one axle with the two sides represented, and the lateral plane, which represents the two axles, but only one side of the vehicle.

Usually, a vehicle has much more symmetry between the sides, rather than the ends. In other words, the Sagittal Plane (that divides the vehicle body in left and right) results in better symmetrical results in contrast to the Coronal Plane (that partitions the body in front and rear).

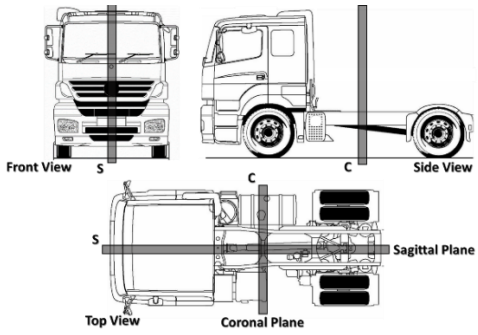

Figure 5. Bilateral Symmetry

As depicted in Figure 5, it is evident that analyzing the half-car model in terms of pitch, considering the rotational degree of freedom of the sprung mass, is relatively simpler due to the moment of inertia being half of the full configuration. However, when studying the roll behavior, determining the appropriate moment of inertia is not as straightforward and requires further consideration.

7 DOF MODEL

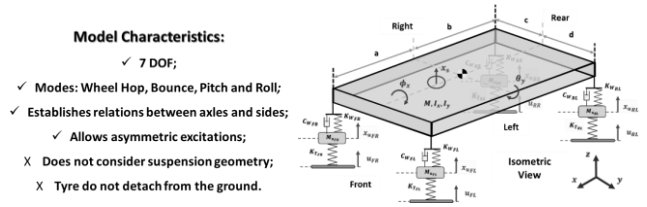

Figure 6. 1/1 Model

ALSO KNOWN AS FULL-CAR – The final MSD model represents both sides and both axles, for the unsprung mass 4 wheel hop modes, and for the sprung mass: pitch, roll and bounce, defining the 7 DOF. The 1/1 model allows the asymmetrical excitations, accounting the influence of the sides and axles that may be excited by forces in phase. The simplification assumptions are equal to all previous methods, such as the not detaching tyre, suspension geometry have zero effect and negligible tyre damping, based on [1].

MECHANICS

In the studies of mechanics, especially in the field of dynamic problems, there are some approaches that can be used to determine equations of motion. In vehicle dynamics applications, two methods stand out in relation to others, Newtonian mechanics and Lagrangian mechanics. In Newton's method, his laws of motion are used to formulate the governing equations of the system, always in terms of forces, making it a vector method. In Lagrange's method, the formulations are given by scalar quantities, and it is a method that uses energy. The main equations for each method involve time (t), force (F), linear momentum (p), kinetic energy (K), potential energy (V), and the Lagrangian operator ($\mathcal{L}$).

$$\text{Newton} \rightarrow \sum_i \vec{F_i} = \frac{\mathrm{d}\vec{p}}{\mathrm{d}t} \tag{3}$$

$$\text{Lagrange} \rightarrow \mathcal{L} = K - V \tag{4}$$

The application contexts of each method may depend on the problem. The Newtonian method may not describe systems in microscales very well, for example, or it may depend on a subjective decision made by the engineer. Generally, for systems with few degrees of freedom, the Newtonian method is easily employed and is usually chosen. However, for systems with a higher number of DOF, the vector notation used in the Newtonian method can become cumbersome, and a scalar method may be preferred, as in the case of Lagrange method.

In the applications discussed in this paper, the equations are presented as follows. In the Newtonian method, mass (m) and acceleration ($\ddot{x}$) are used, whereas in the Lagrangian method, generalized coordinates (q_i) are employed.

$$\text{Newton} \rightarrow \sum F = m \cdot \ddot{x} \tag{5}$$

$$\text{Lagrange} \rightarrow \frac{\mathrm{d}}{\mathrm{d}t}\left(\frac{\partial \mathcal{L}}{\partial \dot{q}_i}\right) - \frac{\partial \mathcal{L}}{\partial q_i} = 0 \tag{6}$$

INTEGRATION METHODS

In systems with more than one degree of freedom, obtaining an analytical solution demands great effort. In such cases, numerical methods tend to be more efficient. Natural problems are inherently dynamic, meaning they vary over time. However, some problems may vary very slowly, allowing for a static treatment. The problems discussed in this article are entirely dynamic, which means that the governing equations involve derivatives and only one independent variable, namely time.

CLASSICAL METHOD – Generally for 1 DOF it is possible to solve the equation by assuming the form of the solution based on the physical system and knowing the same number of initial conditions and the order of the differential equation. Figure 7 provides a schema that illustrates this analytical approach.

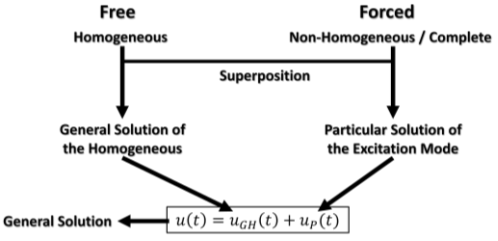

Figure 7. Schematic of Analytical Solution

FINITE DIFFERENCE (FD) – It is an explicit method, meaning that the variable that one wants to find can be written in such a way that it remains alone on one side of the

equation. Figure 8 provides a first visualization of the method.

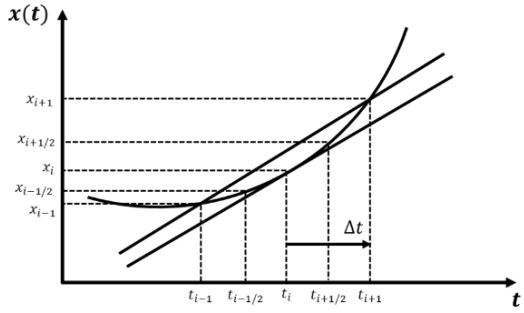

Figure 8. Finite Differences Graphically

The method approximates the first derivative by subtracting the backward Taylor series expansion from the forward series expansion, which are represented by Equations 3 and 4, respectively.

$$x(t_{i-1}) = x(t_i) - h \cdot \dot{x}(t_i) + (2!)^{-1}h^2 \cdot \ddot{x}(t_i) - \cdots \quad (3)$$

$$x(t_{i+1}) = x(t_i) + h \cdot \dot{x}(t_i) + (2!)^{-1}h^2 \cdot \ddot{x}(t_i) + \cdots \quad (4)$$

The first derivative (Equation 5) is obtained by truncating the Taylor series at the first-order, neglecting higher-order terms, the second derivative (Equation 6) is approximated by adding the expansions, for a time step of h.

$$\dot{x}(t_i) = \frac{x(t_{i+1}) - \dot{x}(t_{i-1})}{2h} \quad (5)$$

$$\ddot{x}(t_i) = \frac{x(t_{i+1}) - 2x(t_i) + x(t_i - 1)}{h^2} \quad (6)$$

It is noteworthy that the variation between time intervals is linear for both velocity and acceleration. The finite difference method presents a stability problem due to the duration of the time step h used. This should not be confused with accuracy, which always improves with smaller steps.

RUNGE-KUTTA (RK) – There is a similarity with Euler's method [4], which is a particular case of the family of Runge-Kutta methods, consisting of an expansion of the Taylor series into truncated form. The methods in this family differ in how they compute the derivative of Equation 7.

$$x(t_{k+1}) = x(t_k) + \frac{h}{6}(k_1 + 2k_2 + 2k_3 + k_4) \quad (7)$$

The k_n parameters are calculated as follows.

$$\begin{aligned} k_1 &= f(x(t_k), t_k) \\ k_2 &= f(x(t_k) + 0.5k_1, t_k + 0.5h) \\ k_3 &= f(x(t_k) + 0.5k_2, t_k + 0.5h) \\ k_4 &= f(x(t_k) + k_3, t_k + h) \end{aligned} \quad (8)$$

METHODOLOGIES

ABOUT SOLVING THE MODELS – To organize the modelling procedures of the mass-spring-dampers systems, the flowchart of Figure 9 was sketched to detail the methodology implemented to build the models.

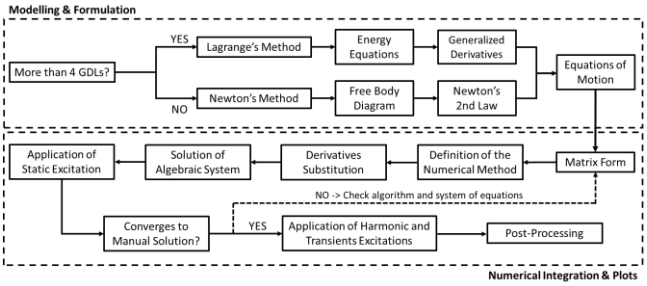

Figure 9. Simulations Fluxogram

The method to obtain the equations of motion is defined based on the number of degrees of freedom of the model. For 7 DOF, the Lagrange method is used and for the others the Newton method is applied.

After the definition of the equations of motion, a matrix form is used administratively to facilitate the method application, then an algorithm can be developed to solve the equations numerically.

A verification of the algorithm and the equations is made by applying a static excitation and then comparing the output response with the theory, since static cases produces a solution that can be calculated manually.

ABOUT THE VEHICLE'S DATA – As the characteristics of the suspension and inertia of the automobile shouldn't matter in terms of how a model performs, Table 1 assigns generic values of a simple vehicle to be used in the phase of model characterization. Hence, all equations of motion have the same constant values, only changing due model's complexity.

Table 1. Vehicle Values for Modelling

Prototype Parameters	Generic Values
Total Mass, M	$240\ kg$
Sprung Mass, M_s	$192\ kg$
Front Axle Unsprung Mass, M_{uF}	$10\ kg/Quarter$
Rear Axle Unsprung Mass, M_{uR}	$14\ kg/Quarter$
Pitch Moment of Inertia, I_θ	$60\ kg.m^2$
Roll Moment of Inertia, I_ϕ	$65\ kg.m^2$
Yaw Moment of Inertia, I_ψ	$70\ kg.m^2$
Wheelbase, L	$1350\ mm$
Front Axle Track Width, T_F	$1350\ mm$
Rear Axle Track Width, T_R	$1250\ mm$
CG Distance to the Front Axle, a	$750\ mm$
CG Distance to the Rear Axle, b	$600\ mm$
CG Lateral Offset	$0\ mm$
Front Wheel Center Rate, K_{wF}	$5\ N/mm$
Rear Wheel Center Rate, K_{wR}	$11\ N/mm$
Front Tyre Vertical Stiffness, K_{TF}	$60\ N/mm$
Rear Tyre Vertical Stiffness, K_{TR}	$70\ N/mm$
Front Suspension Damping, C_{wF}	$320\ N.s/m$
Rear Suspension Damping, C_{wR}	$640\ N.s/m$

MODELLING AND SIMULATIONS

NEWTON'S METHOD & FINITE DIFFERENCES – For the models with low degrees of freedom, due to its complexity, the simple Newton's 2nd Law of Motion can be used together with the FD to solve the models.

Firstly, for the quarter-car model, the following equations of motion (Equation 9) can be written for both sprung and unsprung masses, based on the Free-Body-Diagram (FBD) of Figure 10.

$$M_s\ddot{x}_s + C_w\dot{x}_s + K_w x_s = K_w x_{us} + C_w\dot{x}_{us}$$
$$M_{us}\ddot{x}_{us} + C_w\dot{x}_{us} + (K_w + K_T)x_{us} = C_w\dot{x}_s + K_w x_s + K_T u(t) \quad (9)$$

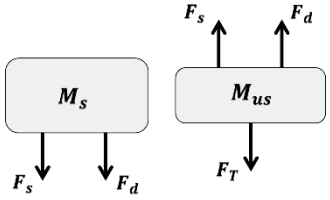

Figure 10. Free-Body Diagram 1/14 Model

Equation 10 shows Equation 9 in the matricial form.

$$\begin{bmatrix} M_s & 0 \\ 0 & M_{us} \end{bmatrix}\begin{Bmatrix} \ddot{x}_s \\ \ddot{x}_{us} \end{Bmatrix} + \begin{bmatrix} C_w & -C_w \\ -C_w & C_w \end{bmatrix}\begin{Bmatrix} \dot{x}_s \\ \dot{x}_{us} \end{Bmatrix} + \begin{bmatrix} K_w & -K_w \\ -K_w & K_w + K_T \end{bmatrix}\begin{Bmatrix} x_s \\ x_{us} \end{Bmatrix} = \begin{Bmatrix} 0 \\ K_T u(t) \end{Bmatrix} \quad (10)$$

As mentioned in the topic of numerical integration, the derivatives are approximated and the differential equations becomes an algebraic equation, that comes from the substitution of the $\dot{x}$ and $\ddot{x}$ terms of Equation 10 with the terms illustrated in Figure 11.

	Sprung Mass	Unsprung Mass:
Discrete Acceleration:	$\ddot{x}_s^i \approx \frac{x_s^{i+1} - 2x_s^i + x_s^{i-1}}{\Delta h^2}$	$\ddot{x}^i{}_{us} \approx \frac{x_{us}^{i+1} - 2x_{us}^i + x_{us}^{i-1}}{\Delta h^2}$
Discrete Velocity:	$\dot{x}_s^i \approx \frac{x_s^{i+1} - x_s^{i-1}}{2\Delta h}$	$\dot{x}_{us}^i \approx \frac{x_{us}^{i+1} - x_{us}^{i-1}}{2\Delta h}$

Evaluations made at time t^i

Figure 11. Approximated Derivatives for 2 DOF

Then, with this explicit method applied, a 2x2 linear system is constructed, Equation 11, and it is solved for every time instant of interest.

$$\begin{Bmatrix} x_s^{i+1} \\ x_{us}^{i+1} \end{Bmatrix} \approx A^{-1}\left(B_1\begin{Bmatrix} 0 \\ u^i \end{Bmatrix} + B_2\begin{Bmatrix} x_s^i \\ x_{us}^i \end{Bmatrix} + B_3\begin{Bmatrix} x_s^{i-1} \\ x_{us}^{i-1} \end{Bmatrix}\right)$$
$$A = \begin{bmatrix} \frac{M_s}{\Delta t^2} + \frac{C_w}{2\Delta t} & -\frac{C_w}{2\Delta t} \\ -\frac{C_w}{2\Delta t} & \frac{M_{us}}{\Delta t^2} + \frac{C_w}{2\Delta t} \end{bmatrix};\ B_1 = \begin{bmatrix} 0 & 0 \\ 0 & K_T \end{bmatrix} \quad (11)$$
$$B_2 = \begin{bmatrix} \frac{2M_s}{\Delta t^2} - K_w & K_w \\ K_w e & \frac{2M_{us}}{\Delta t^2} - (K_w + K_T) \end{bmatrix}$$
$$B_3 = \begin{bmatrix} \frac{C_w}{2\Delta t} - \frac{M_s}{\Delta t^2} & -\frac{C_w}{2\Delta t} \\ -\frac{C_w}{2\Delta t} & \frac{C_w}{2\Delta t} - \frac{M_{us}}{\Delta t^2} \end{bmatrix}$$

The remaining final stage are the initial conditions (IC). A trivial consideration is to define all of them as zero, and since there are 2 second-order differential equations, 4 IC are necessary. Usually, they are defined as the displacements and the velocities at time 0, because with the velocity one can calculate the displacement at the next time step based on the previous value. Figure 12 displays the IC.

$$\text{Initial Conditions:}\quad \begin{matrix} x_s(0) = x_{s_0} \\ x_{us}(0) = x_{us_0} \\ v_s = \dot{x}_s(0) = \dot{x}_{s_0} \\ v_{us} = \dot{x}_{us}(0) = \dot{x}_{us_0} \end{matrix} \longrightarrow \begin{matrix} x_s(1) = v_s \cdot \Delta t + x_{s_0} \\ x_{us}(1) = v_{us} \cdot \Delta t + x_{us_0} \end{matrix}$$

Figure 12. IC for 1/4 Model

In the case of the 1/2 model, the same approach is used, only differing by the number of masses and, consequently, equations as well. Figure 13 shows the FBD of the three masses that composes the half-car.

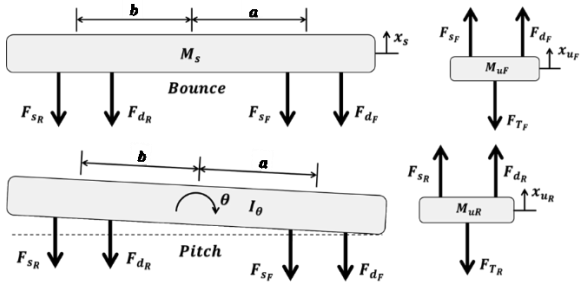

Figure 13. Free-Body Diagram 1/2 Model

The forces that act on springs and dampers are collinear, only having the offset for didactics purposes. Initially, the equations of motion are simply the sum of the forces, as seen in Equation 12.

$$\begin{aligned} M_s \cdot \ddot{x}_s &= -(F_{sF} + F_{dF} + F_{sR} + F_{dR}) \\ I_\theta \cdot \ddot{\theta} &= -a \cdot (F_{sF} + F_{dF}) + b \cdot (F_{sR} + F_{dR}) \\ M_{uF} \cdot \ddot{x}_{uF} &= -(F_{sF} + F_{dF} + F_{TF}) \\ M_{uR} \cdot \ddot{x}_{uR} &= -(F_{sR} + F_{dR} + F_{TR}) \end{aligned} \quad (12)$$

Then, with the definition of each force, such as spring force $F = kx$ and damping forces are $F = c\dot{x}$, each equation expands to the complete DE, the Equation 13 condense all 4 of them.

$$\begin{aligned} &M_s \cdot \ddot{x}_s + C_{w_F}(\dot{x}_s - \dot{x}_{u_F} + \dot{\theta}a) + C_{w_R}(\dot{x}_s - \dot{x}_{u_R} - \dot{\theta}b) \\ &+K_{w_F}(x_s - x_{u_F} + \theta a) + K_{w_R}(x_s - x_{u_R} - \theta b) = 0 \\ &I_\theta \cdot \ddot{\theta} + C_{wF}a(\dot{x}_s - \dot{x}_{u_F} + \dot{\theta}a) - C_{wR}b(\dot{x}_s - \dot{x}_{u_R} - \dot{\theta}b) \\ &+K_{w_F}a(x_s - x_{u_F} + \theta a) - K_{w_R}b(x_s - x_{u_R} - \theta b) = 0 \\ &M_{u_F} \cdot \ddot{x}_{u_F} - C_{wF}(\dot{x}_s - \dot{x}_{u_F} + \dot{\theta}a) - K_{wF}(x_s - x_{u_F} + \theta a) \\ &+ K_{T_F}(x_{uF} - u_1) = 0 \\ &M_{u_R} \cdot \ddot{x}_{u_R} - C_{wR}(\dot{x}_s - \dot{x}_{u_R} - \dot{\theta}b) - K_{wR}(x_s - x_{u_F} - \theta b) \\ &+ K_{T_R}(x_{uR} - u_2) = 0 \end{aligned} \quad (13)$$

With the same methodology used for the quarter-car, the derivatives are approximated via finite differences, resulting in the Equation 14.

$$\begin{Bmatrix} x_S^{i+1} \\ \theta^{i+1} \\ x_{uF} \\ x_{uR} \end{Bmatrix} \approx A^{-1}\left([B_1]\{E^i\} + [B_2]\{d^i\} + [B_3]\{d^{i-1}\}\right)$$

$$A = \begin{bmatrix} -M - C_F - C_R & C_F a - C_R b & C_F & C_R \\ C_F a - C_R b & -I - C_F a^2 - C_R b^2 & -C_F a & C_R b \\ C_F & -C_F a & -M_F - C_F & 0 \\ C_R & C_R b & 0 & -M_R - C_R \end{bmatrix}$$

$$B_1 = \begin{bmatrix} 0 & 0 & 0 & 0 \\ 0 & 0 & 0 & 0 \\ 0 & 0 & -K_{T_F} & 0 \\ 0 & 0 & 0 & -K_{T_R} \end{bmatrix} \quad (14)$$

$$B_2 = \begin{bmatrix} K_{wF} + K_{wR} - 2M & K_{wR} b - K_{wF} a & -K_{wF} & K_{wR} \\ K_{wR} b - K_{wF} a & K_{wR} b^2 + K_{wF} a^2 - 2I & K_{wF} a & -K_{wR} b \\ -K_{wF} & K_{wF} a & K_{wF} + K_{T_F} - 2M_F & 0 \\ -K_{wR} & K_{wR} b & 0 & K_{wR} + K_{TR} - 2M_R \end{bmatrix}$$

$$B_3 = \begin{bmatrix} M - C_F - C_R & C_F a - C_R b & C_F & C_R \\ C_F a - C_R b & I - C_F a^2 - C_R b^2 & -C_F a & C_R b \\ C_F & -C_F a & M_F - C_F & 0 \\ C_R & C_R b & 0 & M_R - C_R \end{bmatrix}$$

The 4x4 linear system have the following parameters.

- $h \rightarrow$ Time step;
- $A, B_1, B_2, B_3 \rightarrow$ Auxiliary Matrices;
- $E^i \rightarrow$ Column Vector of Excitations;
- $d^i \rightarrow$ Column Vector of Displacements Evaluated at $t = i$;
- $d^{i-1} \rightarrow$ Column Vector of Displacements Evaluated at $t = i$;

And the parameters for simplified notation.

$$\frac{M_{u_F}}{\Delta t^2} = M_F \qquad \frac{C_{w_F}}{2\Delta t} = C_F$$

$$\frac{M_s}{\Delta t^2} = M$$

$$\frac{M_{u_R}}{\Delta t^2} = M_R \qquad \frac{C_{w_R}}{2\Delta t} = C_R$$

The IC have the identical definition as previous model, so it would not be explicit defined once again.

LAGRAGIAN METHOD & RUNGE-KUTTA – For the last model, with 7 DOF, the approach used so far is not so convenient. Even for a medium model, such as the half-car, the equations are sufficient large to not be well accommodated.

Figure 14 provides the fundamental equation to be applied in this method. Only with the definition of the 3 energy equations, the equations of motion can be written directly with the following formula.

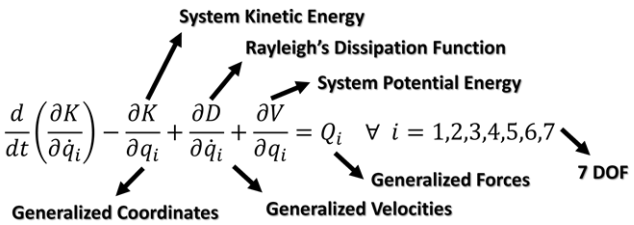

Figure 14. Lagrange Method for 7 DOF

The kinetic, potential and dissipation energies are defined by Equations 15, 16, 17.

$$K = \frac{1}{2}M\dot{x_s}^2 + \frac{1}{2}I_x\dot{\phi}^2 + \frac{1}{2}I_y\,\dot{\theta}^2 + \frac{1}{2}M_{uF}\left(\dot{x}_{u_{FL}}^2 + \dot{x}_{u_{FR}}^2\right) + \frac{1}{2}M_{uR}\left(\dot{x}_{u_{RR}}^2 + \dot{x}_{u_{RL}}^2\right) \quad (15)$$

$$V = \frac{1}{2}K_{wF}\left(x_s - x_{u_{FL}} + d\phi - a\theta\right)^2 + \frac{1}{2}K_{wF}\left(x_s - x_{u_{FR}} - c\phi - a\theta\right)^2 + \frac{1}{2}K_{wR}\left(x_s - x_{u_{RL}} - d\phi + b\theta\right)^2 + \frac{1}{2}K_{wR}\left(x_s - x_{u_{RR}} + c\phi + b\theta\right)^2 + K_{TF}\left(x_{u_{FL}} - u_{FL}\right)^2 + \frac{1}{2}K_{TF}\left(x_{u_{FR}} - u_{FR}\right)^2 + K_{TR}\left(x_{u_{RL}} - u_{RL}\right)^2 + \frac{1}{2}K_{TR}\left(x_{u_{RR}} - u_{RR}\right)^2 \quad (16)$$

$$D = \frac{1}{2}C_{wF}\left(\dot{x}_s - \dot{x}_{u_{FL}} + d\dot{\phi} - a\dot{\theta}\right)^2 + \frac{1}{2}C_{wF}\left(\dot{x}_s - \dot{x}_{u_{FR}} - c\dot{\phi} - a\dot{\theta}\right)^2 + \frac{1}{2}C_{wR}\left(\dot{x}_s - \dot{x}_{u_{RL}} - d\dot{\phi} + b\dot{\theta}\right)^2 + \frac{1}{2}C_{wR}\left(\dot{x}_s - \dot{x}_{u_{RR}} + c\dot{\phi} + b\dot{\theta}\right)^2 \quad (17)$$

With Equations 15 to 17 properly defined, it is possible to write the equations of motion using Lagrange's equation by taking partial derivatives of the energy formulation with respect to each degree of freedom (DOF), one by one. Reference [1] provides the equations of motion and Equation 18 shows them without an anti-roll bar.

$$\begin{bmatrix} M & 0 & 0 & 0 & 0 & 0 & 0 \\ 0 & I_y & 0 & 0 & 0 & 0 & 0 \\ 0 & 0 & I_x & 0 & 0 & 0 & 0 \\ 0 & 0 & 0 & M_{u_F} & 0 & 0 & 0 \\ 0 & 0 & 0 & 0 & M_{u_F} & 0 & 0 \\ 0 & 0 & 0 & 0 & 0 & M_{u_R} & 0 \\ 0 & 0 & 0 & 0 & 0 & 0 & M_{u_R} \end{bmatrix} \begin{Bmatrix} \ddot{x}_s \\ \ddot{\phi} \\ \ddot{\theta} \\ \ddot{x}_{u_{FL}} \\ \ddot{x}_{u_{FR}} \\ \ddot{x}_{u_{RR}} \\ \ddot{x}_{u_{RL}} \end{Bmatrix} + \begin{bmatrix} 2(C_{wF} + C_{wR}) & c_{12} & c_{13} & -C_{wF} & -C_{wF} & -C_{wR} & -C_{wR} \\ c_{21} & c_{22} & c_{23} & -dC_{wF} & cC_{wF} & dC_{wR} & -cC_{wR} \\ c_{31} & c_{32} & c_{33} & aC_{wF} & aC_{wF} & -bC_{wR} & -bC_{wR} \\ -C_{wF} & -dC_{wF} & aC_{wF} & C_{wF} & 0 & 0 & 0 \\ -C_{wF} & cC_{wF} & aC_{wF} & 0 & C_{wF} & 0 & 0 \\ -C_{wR} & dC_{wR} & -bC_{wR} & 0 & 0 & C_{wR} & 0 \\ -C_{wR} & -cC_{wR} & -bC_{wR} & 0 & 0 & 0 & C_{wR} \end{bmatrix} \begin{Bmatrix} \dot{x}_s \\ \dot{\phi} \\ \dot{\theta} \\ \dot{x}_{u_{FL}} \\ \dot{x}_{u_{FR}} \\ \dot{x}_{u_{RR}} \\ \dot{x}_{u_{RL}} \end{Bmatrix} +$$

$$+ \begin{bmatrix} 2(K_{wF} + K_{wR}) & k_{12} & k_{13} & -K_{wF} & -K_{wF} & -K_{wR} & -K_{wR} \\ k_{21} & k_{22} & k_{23} & -dK_{wF} & cK_{wF} & dK_{wR} & -cK_{wR} \\ k_{31} & k_{32} & k_{33} & aK_{wF} & aK_{wF} & -bK_{wR} & -bK_{wR} \\ -K_{wF} & -dK_{wF} & aK_{wF} & K_{wF} + K_{TF} & 0 & 0 & 0 \\ -K_{wF} & cK_{wF} & aK_{wF} & 0 & K_{wF} + K_{TF} & 0 & 0 \\ -K_{wR} & dK_{wR} & -bK_{wR} & 0 & 0 & K_{wR} + K_{TR} & 0 \\ -K_{wR} & -cK_{wR} & -bK_{wR} & 0 & 0 & 0 & K_{wR} + K_{TR} \end{bmatrix} \begin{Bmatrix} x_s \\ \phi \\ \theta \\ x_{u_{FL}} \\ x_{u_{FR}} \\ x_{u_{RR}} \\ x_{u_{RL}} \end{Bmatrix} = \begin{bmatrix} 0 \\ 0 \\ 0 \\ K_{TF}u_{FL} \\ K_{TF}u_{FR} \\ K_{TR}u_{RR} \\ K_{TR}u_{RL} \end{bmatrix} \quad (18)$$

Some operations were condensed in a single parameter to help the notation. Those parameters are defined next.

$$k_{12} = k_{21} = K_{wF}(d - c) + K_{wR}(c - d) \qquad c_{12} = c_{21} = C_{wF}(d - c) + C_{wR}(c - d)$$
$$k_{13} = k_{31} = 2(bK_{wR} - aK_{wF}) \qquad c_{13} = c_{31} = 2(bC_{wR} - aC_{wF})$$
$$k_{23} = k_{32} = K_{wF}(ac - ad) + K_{wR}(bc - bd) \qquad c_{23} = c_{32} = C_{wF}(ac - ad) + C_{wR}(bc - bd)$$
$$k_{22} = (K_{wF} + K_{wR})(d^2 + c^2) \qquad c_{22} = (C_{wF} + C_{wR})(d^2 + c^2)$$
$$k_{33} = 2(K_{wF}a^2 + K_{wR}b^2) \qquad c_{33} = 2(C_{wF}a^2 + C_{wR}b^2)$$

To solve the equations, it is better to do it computationally only, writing them directly in the format of the chosen solver, in this case the Runge-Kutta of 4th order, also named as Dormand-Prince, which is a medium order method.

At this point, all the models were already formulated with the equations of motion defined and the method of numerical integration selected.

VERIFICATION – Before comparing the models, the algebraic equations and/or integration algorithms (python was used) must be tested for verification and to ensure that the modeling accurately represents the mechanical systems of MSD. The concern lies in accurately modeling the systems, without aiming necessarily for a realistic representation at this point (this will be addressed in the conclusion section). This paper focuses on the validation of models that justify the use of custom-developed algorithms.

For the 1/4 model, a pseudo-static load is applied in an, although simpler, equivalent system, Figure 15. The "pseudo" part it's because it's applied as an impact, and the "static" one due to converges to the same final static

displacement. The stiffness and damping are simplified, the latter only accelerates the convergence.

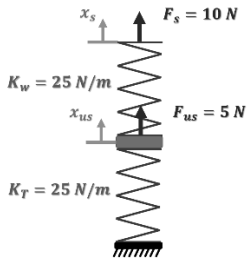

Figure 15. System for Static Validation - 2 DOF

The 2 displacements after the equilibrium is reestablished are calculated with simple static mechanics.

$$x_{us} = \frac{F_s + F_{us}}{K_T} = \frac{15}{25} = 0.6\ m$$
$$x_s = \frac{F_s}{K_w} + x_{us} = \frac{10}{25} + 0.6 = 1.0\ m \tag{19}$$

Equation 19 provides the analytical and exact solution of the problem. Figure 16 displays the response of the code, which agrees with the predicted values, demonstrating the coherence of all development for this model.

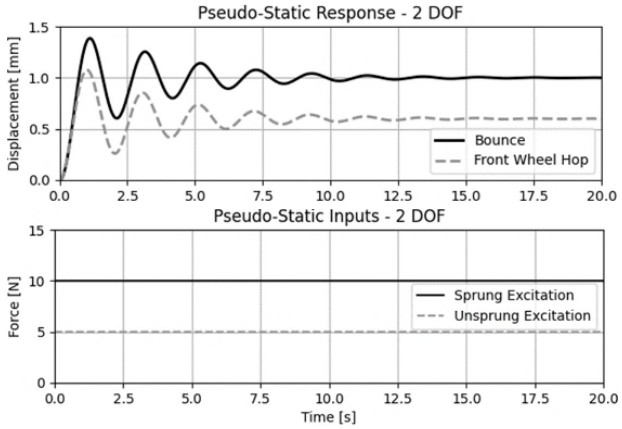

Figure 16. Pseudo-Static Validation of Quarter-Car Model

The same reasoning applies to the 4 DOF model, where a simplified approach is employed. In this case, a quasi-static load is applied, consisting of a 1 N force exerted over a 60-second period. This loading condition ensures minimal introduction of inertial effects.

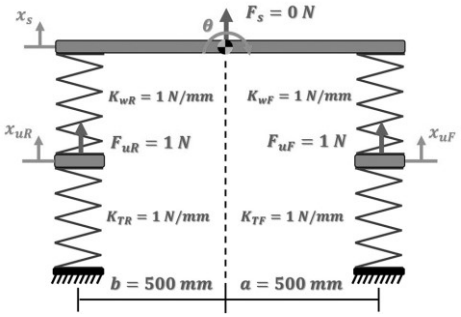

Figure 17. System for Static Validation - 4 DOF

As the parameters of stiffness and forces are all unitary, all translational DOF must equal one, and the rotational must be null ($a = b$). Figure 18 displays the response obtained.

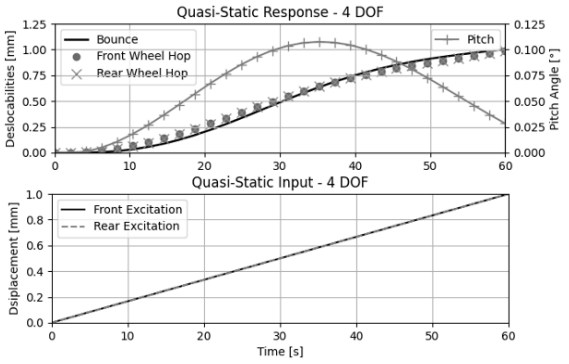

Figure 18. Static Validation of Half-Car

Both bounce and wheel hops are calculated precisely by the algorithm, and a very good response is obtained for the pitch angle, that should be always zero, but since the calculus is made in radians, the actual calculated max value is $2 \cdot 10^{-3}$.

Another methodology that can be used to validate the formulation and the algorithm is to set an initial condition of displacement in the sprung mass of 100 mm, and release it in free vibration, without road inputs. Then, with the Fast Fourier Transform (FFT) the main frequency of the signal can be calculated and compared with the natural frequency of the modal analysis.

First, Figure 19 shows the free response and the corresponding FFT of the bounce subcritical damping curve.

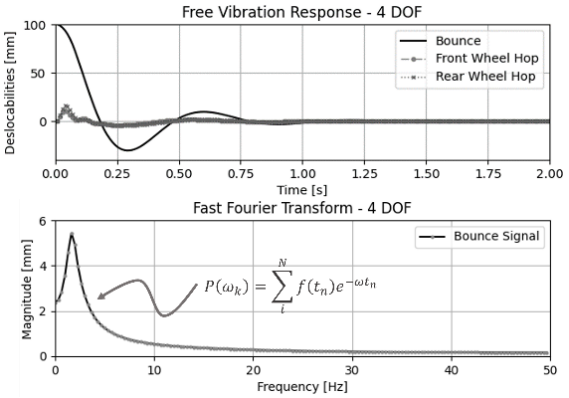

Figure 19. Free Vibration Validation of Half-Car

The damping ratio ζ can be predicted and estimated simply by counting the number of cycles in the curve. The physical meaning of ζ is the percentage of energy that is dissipated in one cycle, since there are 3 peaks in the signal, the damping ratio is around $33.\overline{3}\%$. The main frequency of the spectrum plotted is $1.66\ Hz$.

Through the modal analysis, the natural frequency for the first mode of vibration is $1.77\ Hz$, and the damped one is $1.68\ Hz$, giving a damping ratio ζ_1 of 31%.

$$\det([K] - \omega^2[M]) = 0$$
$$f_{n_1} = 1.77\ Hz$$
$$\det([-M]^{-1}[K] - [M]^{-1}[C] - \omega^2[I]) = 0 \tag{20}$$
$$f_{d_1} = 1.68\ Hz$$

The second verification is completed successfully. Since the 7 DOF behaves just like a 4 DOF when excited symmetrically by the sides, its validation is made by comparing the response of both models. This justifies the use of 2 methods to assure a good representative 4 DOF modelling, that consequently assures the good 7 DOF as well.

Figure 20 provides the response of the algorithm developed for the 7 DOF modelled previously with Runge-Kutta, along the 4 DOF curves. Primarily, the half-car was solved with finite differences, which showed a disparity with the 7 DOF, so a RK solver was also implemented to check that the variation is only due to the numerical method. The input of the road used was a step of 100 mm of height at time $t = 1.0\ s$.

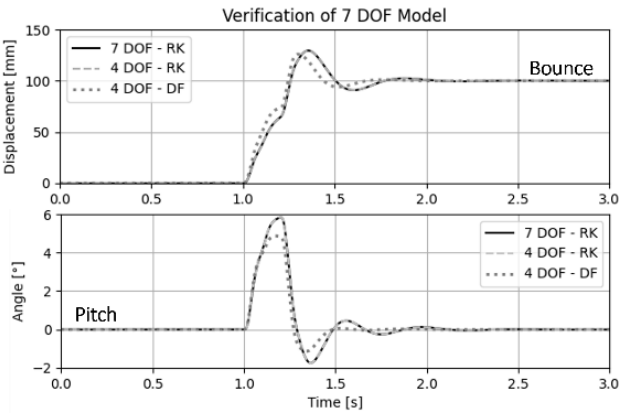

Figure 20. Validation of Full-Car

Finally, all the equations of motion and algorithms were checked to assure that the models and solvers truly represent the MSD systems.

RESULTS AND DISCUSSIONS

MODAL ANALYSIS – Naturally, as the number of modes considered increases, the natural frequency of the sprung mass decreases. Table 2 presents all natural frequencies of each model.

Table 2. Natural Frequencies Comparison

Modal Analysis					
Mode / Model	Bounce	Roll	Pitch	Front WH	Rear WH
1 DOF	2.0547	*N/A*	*N/A*	*N/A*	*N/A*
2 DOF	1.9063	*N/A*	*N/A*	12.1302	13.7936
4 DOF	1.7724	*N/A*	2.3721	12.1423	12.8428
7 DOF	1.3356	2.0229	2.3250	12.1330	12.8390

The 1/8 of a car has its natural frequency calculated using the equation of a 1 DOF system, $f_n = 0.159\sqrt{k_w/m_s}$. This value corresponds to the classical application, where it represents only the sprung mass on one side of the car. In the 1/4 model, the same classical approach is used, employing two models: one for the front axle and another for the rear axle, with half of the masses of each axle considered in the calculation. In this approach, there is a very satisfactory characterization in terms of the natural frequency of wheel hop mode.

Considering the full car as reference, doubling the number of degrees of freedom improves the coherence of the natural frequency by approximately 10%.

Table 3. First Mode Difference

Bounce Frequency	
Model	Delta
1 DOF	54%
2 DOF	43%
4 DOF	33%
7 DOF	*Ref.*

An alternative 2 DOF model, Figure 21, that do not represent the unsprung masses (consequently wheel hop mode is not considered) and does calculates pitch mode is analysed. Bounce frequency is 1.85 Hz (delta of 39% from reference), which is not a relevant improvement, but the pitch frequency is 2.55 Hz (delta of only 6% from 7 DOF).

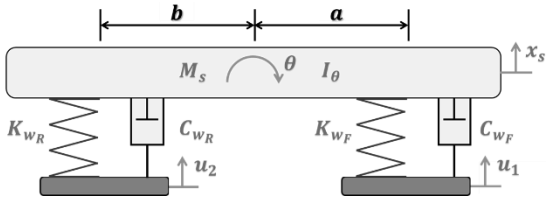

Figure 21. Bounce and Pitch Model

TIME DOMAIN – Naturally, the most straightforward analysis that can be performed is to plot the vertical dynamics models together, using the curves for 1, 2 (only and always for the quarter-car), 4, and 7 degrees of freedom. In the cases of eighth-car and quarter-car models, both are solved two times with data from each axle, allowing to compare more completely.

To facilitate the analysis, a deterministic approach is used to represent road roughness or obstacles, but it's also interesting to use ISO 8608 standard to input representative pavements. Figures 22 and 23 shows the response of a transient input at time $t = 1.0\ s$ in the front axle, and considering a velocity around 25 km/h, at time $t = 1.2\ s$ in the rear axle, with an amplitude of 100 mm.

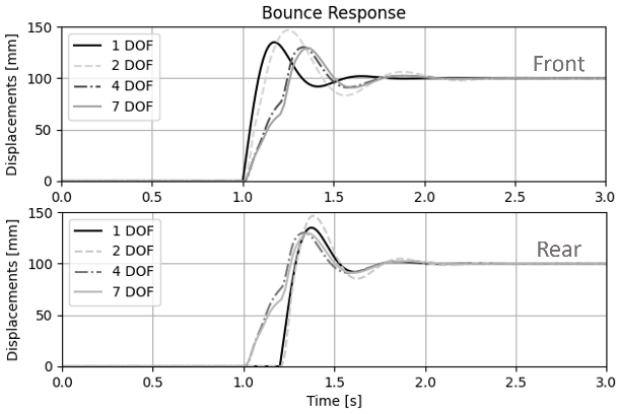

Figure 22. Comparison Between Bounce Mode

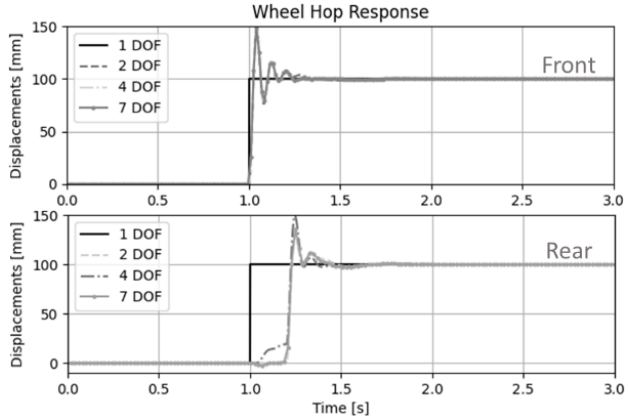

Figure 23. Comparison Between WH Modes

Important to notice that FD was used for the 4 DOF, only to detach from the RK of the 7 DOF and showing the difference of the two methods, otherwise, as the input is symmetrical, both would be always the same. Also, for the 1 DOF, equations of the reference [5] provides the curves plotted above. At last, the response given by 1 and 2 DOF models are obtained at the plane that contains the wheel center of the axles, while models with 4 and 7 DOF returns the displacements at the center of gravity (CG).

Due to the location distance of the point where the displacement is calculated, there is an offset between 1 and 2 DOF in relation to 4 and 7 DOF, although a good amplitude correlation can be seen. The front wheel hop response is almost equal for every model, apart from the 1 DOF, that follows the road input. The rear WH have a good agreement between 7 and 2 DOF, with the half-car model, unexpectedly, diverging from it with the FD, showing a numerical method sensitivity.

For a periodical excitation, 2 quantities must be specified, frequency and amplitude. It was chosen 10 Hz of frequency, so it is close to the WH resonance, and 70 mm of amplitude, a relatively severe road roughness. In this way, an appropriate response to evaluate the models among themselves is generated, with reasonable amplitudes and curves that allow for a good comparative basis, as Figure 24 shows it.

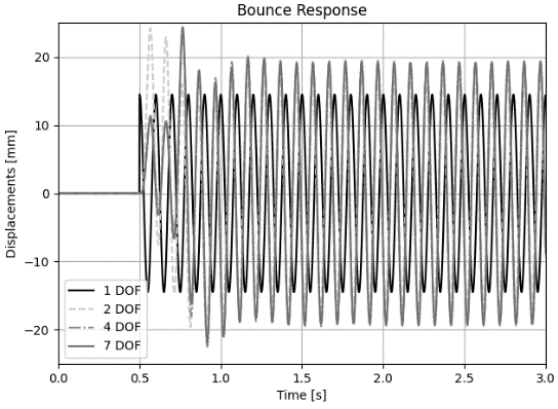

Figure 24. Bounce for Harmonic Input

The response for the wheel hop mode is equal to every model, apart from the 1 DOF. Sprung mass displacement only differs a little in terms of amplitude between quarter-car and the models with more DOF during steady state vibration and differing considerably during the transient portion. For the 1 DOF, the output stays out of phase, with an underestimated amplitude. The input started at 0.5 to check coherence of the response.

CONCLUSIONS

It has been observed that in terms of the natural frequency of the sprung mass, a careful consideration of the more simplified models is necessary. Their natural frequencies do not appropriately characterize the sprung mass, only when taken in their respective analysed axles. For the natural frequencies of the unsprung masses, the simpler 2 DOF model proves to be sufficient.

Regarding the time-domain response, greater versatility is seen in the 4 and 7 DOF models as they enable the possibility of having displacements for the entire sprung mass, using trigonometry. The calculation in the eighth- and quarter-car model is restricted only to the plane of each axle. However, it still exhibits considerable coherence with the more complex models and it is necessary, for example, to obtain the suspension travel over time, which is crucial for structural calculation and for the suspension field of study itself.

It is recommended to maintain the half- and full-car models for scenarios where data of pitch, roll, or displacement at a specific position of the sprung mass is truly necessary. It is also relevant when the natural frequencies of the sprung mass need to be determined, not just those of each individual axle. The frequencies obtained from the quarter-car model, despite deviating from the overall bounce frequency, are important for mitigating pitching vibration when the axles are excited out of phase. The Olley criteria suggests that for comfort, it is desirable to maintain a 30% higher natural frequency of the rear sprung mass compared to the front to reduce the most uncomfortable mode of vibration, pitch (subjectively), according to reference [3].

These models serve various purposes, including the analysis of macro behaviours, trend analysis, rapid data acquisition of physical quantities, the design of simple vehicles, and the introduction of the field of study in dynamics. Considering the last statement, this paper aimed to provide pertinent information about the models and their comparative performance, facilitating the selection of the most suitable model for the intended application.

NEXT-STEPS – The natural course to take after this paper is to extend the comparison, including more models, more numerical methods, tyre damping sensitivity, different road excitations, a multibody analysis, an experimental result with vehicle data, and then attaching all together.

CONTACT

Paulo Henrique Dayrell Drummond de Oliveira
paulo.drummond01@gmail.com

REFERENCES

[1] JAZAR, R. N. (2008). Vehicle Dynamics (Vol.1). New York: Springer.

[2] MILLIKEN, W. F., Milliken, D. L., & Metz, L. D. (1995). Race Car Vehicle Dynamics (Vol. 400). Warrendale: SAE International.

[3] GILLESPIE, T. D. (1992). Fundamentals of Vehicle Dynamics. Society of Automotive Engineers. Inc, 400, 15096-0001.

[4] BOYCE, W. E., & DiPRIMA, R. C. (2020). Equações Diferenciais Ordinárias e Problemas de Valores de Contorno. São Paulo: Livros Técnicos e Científicos (LTC).

[5] BALACHANDRAN, B., & Magrab, E. B. (2018). Vibrations. Cambridge University Press.

[6] OLIVEIRA, P. H. D. D. de. (2022). Desenvolvimento de Modelos Computacionais em Termos de Dinâmica Veicular. UFJF.